Liquid Crystal Leaky-Wave Antennas With Dispersion Sensitivity Enhancement

Shuang Ma, Guo-Hui Yang, *Member, IEEE*, Daniel Erni, *Member, IEEE*, Fan-Yi Meng, *Senior Member, IEEE*, Lei Zhu, Qun Wu, *Senior Member, IEEE*, and Jia-Hui Fu, *Senior Member, IEEE*

***Abstract*— A novel design, fabrication, and packaging technology is proposed for liquid crystal (LC)-based beam-scanning leaky-wave antennas (LWAs). Different from conventional ones, extra dispersion sensitivity enhancement (DSE) components are introduced to increase the slope of effective phase constant versus frequency of LWAs and, hence, the beam scanning range. CST MW Studio software package is used to validate the design method. It is shown that, by adding the DSE components, the electrical beam scanning range is extended by more than 56% in the Ku satellite communication band, where good impedance matching and balanced condition are kept for both extreme tuning states of LCs. Prototypes of the designed LC-composite right/left-handed LWAs with and without the DSE components are fabricated and measured. The fabrication methodology incorporating printed circuit board and precision metal processing technology ensures the mechanical stability, flexible design, perfect packaging, and low cost. Finally, the feature-selective validation technique validates that the measured and simulated results are in good agreement.**

***Index Terms*— Beam scanning, composite right/left-handed (CRLH), dispersion sensitivity enhancement (DSE), fabrication methodology, leaky-wave antenna (LWA), liquid crystal (LC).**

I. Introduction

LEAKY-WAVE antennas (LWAs) have been widely investigated in the past decades due to their unique characteristics, such as narrow and directive beams, comparatively low profile, as well as an inherently simple feeding network [1]–[3]. Particularly, LWAs with beam steering capability employed in the Ku satellite communication band are able to increase the channel capacity significantly and improve communication quality. While compared to the phased-array antennas, LWAs provide a simple solution with compact size, low cost, and ease of integration. However, traditional LWAs are not able to steer beams for a fixed frequency; thus, they need a wide frequency band and waste the increasingly limited spectrum resources [4]–[6]. To solve this issue, fixed-frequency LWAs with tunable beams are investigated adopting ferrite, varactor, and liquid crystal (LC). The ferrite is widely applied in tunable microwave devices with high tuning speed and wide tuning performance, but its loss is very high [7], [8]. On the other hand, varactors are taken as substitution in some cases for their relatively low loss and flexible mechanism [9], [10], but their operating frequency is usually limited below 10 GHz due to the large parasitics of packaging.

LCs are a potential candidate for tunable LWAs at high frequency due to their controllable dielectric parameters and low loss property. The relative permittivity of LCs can be described in terms of the order tensor, normally a uniaxial tensor with nonzero principal components $\varepsilon_{r\perp}$ and $\varepsilon_{r//}$ corresponding to the relative permittivity in the normal and parallel directions of the director with respect to the applied bias field, respectively [11]. The continuously variable permittivity exhibited by LCs leads to the development of reconfigurable antennas and microwave devices [12]–[14]. In the case of LCs-based LWAs, as the permittivity of LCs is tuned by a bias electric field (or voltage), the phase constant and radiation direction of LWAs can be steered [15]–[18].

However, the tunable LC-LWAs suffer from a narrow beam scanning range due to the restricted tunability of the LC permittivity. This phenomenon seriously affects the quality of satellite communication, which leads to the LC-LWAs being difficult to be widely applied in practice. For instance, the beam-scanning angle range of LC-composite right/left-handed (CRLH) LWAs only achieves 14° and 15° at 26.7 GHz in [15] and [17], respectively. Although the scanning range was further extended to 40° by optimizing the feeding structure in [16], there is still lack of a general method to enlarge the beam scanning range of LC-LWAs. Therefore, how to improve the scanning range of the Ku-band LC-LWAs has become a key problem to be urgently solved.

Moreover, the LCs are liquid materials, which leads to complicated design and difficult packaging for microwave components. Most of the existing LC microwave devices are processed by microelectronic technology [15]–[18], which makes the project of the microwave devices limited and increases the process cost [19].

From this point, in this paper, we propose a novel dispersion sensitivity enhancement (DSE) method to enlarge

Manuscript received December 5, 2016; revised January 20, 2017; accepted February 28, 2017. Date of publication April 4, 2017; date of current version May 15, 2017. This work was supported in part by the National Natural Science Fund of China under Grant 61671180 and Grant 61501275, in part by the Science Foundation Project of Heilongjiang Province of China, under Grant QC2015073, and in part by the Deutsche Forschungsgemeinschaft in the framework of DFG CRC/TRR 196 MARIE. Recommended for publication by Associate Editor A. Orlandi upon evaluation of reviewers' comments. *(Corresponding author: Fan-Yi Meng.)*

S. Ma, G.-H. Yang, F.-Y. Meng, Q. Wu, and J.-H. Fu are with the Department of Microwave Engineering, Harbin Institute of Technology, Harbin 150001, China (e-mail: 14B905003@hit.edu.cn; gh.yang@hit.edu.cn; fymenghit@gmail.com; qwu@hit.edu.cn; fjh@hit.edu.cn).

D. Erni is with the Laboratory for General and Theoretical Electrical Engineering (ATE), Center for Nanointegration Duisburg–Essen (CENIDE), Faculty of Engineering, University of Duisburg–Essen, 47048 Duisburg, Germany (e-mail: daniel.erni@uni-due.de).

L. Zhu is with the Institute of Communication and Electronics Engineering, Qiqihar University, Qiqihar 161006, China (e-mail: zhuzhubutterfly@163.com)

Color versions of one or more of the figures in this paper are available online at http://ieeexplore.ieee.org.

Digital Object Identifier 10.1109/TCPMT.2017.2683529

the beam scanning range of CRLH-LWAs. The LCs are introduced and packaged through printed circuit board (PCB) and precision metal processing technology. This new type of fabrication methodology ensures the LC components' low cost and the mechanical stability. Moreover, the electrical beam scanning range is enhanced by the DSE method. Theoretical predictions, numerical simulation results, and experimental results are in good agreement. The approach presented in this paper offers a new way for the design fabrication and packaging of wide-angle beam-scanning LC-CRLH-LWAs.

II. Theoretical Description for DSE Method

For CRLH-LWAs, the main beam direction θ is determined by the phase constant β of the guided wave structure. Let us assume that the maximum and minimum tunable effective permittivities of the LCs correspond to the phase constants β_1 and β_2, and the main beam direction θ_1 and θ_2 of the LC-CRLH-LWA, respectively. Thus, the electrical beam scanning range of the LC-CRLH-LWA can be calculated by

$$\Delta\theta = \theta_1 - \theta_2 = \arcsin\frac{\beta_1}{k_0} - \arcsin\frac{\beta_2}{k_0} \tag{1}$$

where k_0 is the wavenumber in free space. It can be seen that increasing the difference between β_1 and β_2 can enlarge the beam scanning range $\Delta\theta$ of the LC-CRLH-LWA due to the monotony of the inverse sine function. Fig. 1 shows the frequency dependence of LC-CRLH-LWA phase constants under two extreme states of LCs (corresponding to the minimum and maximum effective permittivity of the LCs, respectively). Line 1 with the slope a_1 describes β_1 for the state of the maximum LCs' effective permittivity, and Line 2 with the slope a_2 represents β_2 for the minimum LCs' effective permittivity (a_1 and a_2 can be equal or not). Here, the frequency response of β is assumed to be linear (i.e., the LWA is dispersionless) [7], [20], [21]. The antenna is under balanced states for both the two extreme states of LCs, and the balanced angular frequencies are ω_1 and ω_2.

In most cases, broadside radiation is desirable for LWAs, which leads to an operating angular frequency ω_0 between ω_1 and ω_2 (i.e., $\omega_2 > \omega_0 > \omega_1$), as shown in Fig. 1. Consequently, the increase of a_1 or a_2 causes a larger difference between β_1 and β_2, hence a wider electrical beam scanning range. Based on the analysis, enhancing the dispersion sensitivity of LC-CRLH- LWAs turns out to be an effective but demanding way to expand the beam scanning range.

Existing methods of enhancing the dispersion sensitivity are limited by practical fabrication and design techniques [7], [22], [23]. The LC-CRLH-LWA is usually composed of periodically arranged unit cells. The dispersion sensitivity of this LC-CRLH-LWA can be expressed as the derivative of β_{CRLH} with respect to the angular frequency

$$\frac{d\beta_{\mathrm{CRLH}}}{d\omega} = \frac{1}{d}\sqrt{L_R C_R} + \frac{1}{\omega^2 d\sqrt{L_L C_L}} \tag{2}$$

where d is the total length of the overall unit cell; additionally, L_R/C_L and C_R/L_L represent the right-handed (RH)/ left-handed (LH) distributed series inductance/capacitance

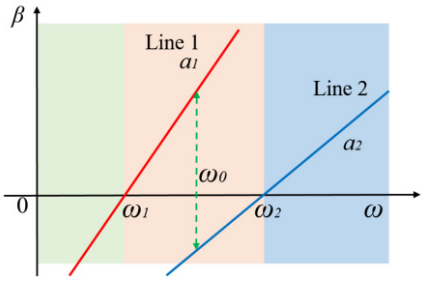

Fig. 1. Dispersion diagram of an LC-CRLH-LWA for two extreme states of LCs.

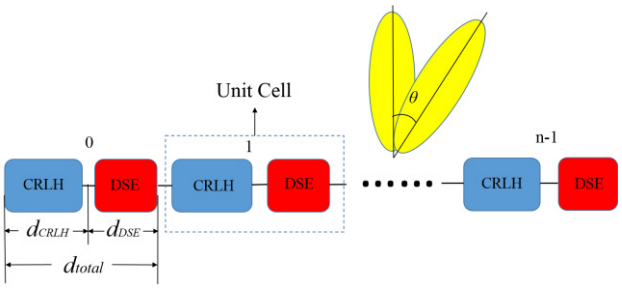

Fig. 2. Schematic of the LC-CRLH-LWA with the inclusion of DSE components.

and shunt capacitance/inductance, respectively. Meanwhile, the LC-CRLH-LWA needs to satisfy the following balanced condition as:

$$\sqrt{L_L/C_L} = \sqrt{L_R/C_R}. \tag{3}$$

In this case, the balanced angular frequency is

$$\omega_0 = \frac{1}{\sqrt{L_R C_L}} = \frac{1}{\sqrt{L_L C_R}}. \tag{4}$$

According to (2), increasing L_R or C_R can enhance the dispersion sensitivity. However, according to (3) and (4), L_R, C_R, C_L, and L_L must change harmonically in order to keep the balanced condition and thus the balanced frequency constant. In many cases, such design requirement is hard to satisfy, as one has to make a tradeoff between the performance and the feasibility. Taking the microstrip transmission line for an example, only very narrow strips can produce large distributed series inductance L_R, but the narrow strips decrease the distributed shunt capacitance C_R. Although the decrease of C_R can be complemented by adopting a thinner substrate, the thickness of the substrate is limited by the practical PCB technology.

In this case, a novel effective and general method to enhance electrically tunable beam scanning range of CRLH-LWAs is anticipated. In fact, the dispersion sensitivity of the CRLH-LWA can be increased by introducing extra DSE components with high dispersion sensitivity, as sketched in Fig. 2. The effective phase constant of the new unit cell, including the CRLH cell and the DSE component, can be expressed as

$$\begin{aligned}\beta_{\mathrm{CRLH-DSE}}(\omega) &= \frac{\phi_{\mathrm{CRLH}}(\omega) + \phi_{\mathrm{DSE}}(\omega)}{d_{\mathrm{total}}} \\ &= \frac{\phi_{\mathrm{CRLH}}(\omega) + \phi_{\mathrm{DSE}}(\omega)}{d_{\mathrm{CRLH}} + d_{\mathrm{DSE}}}\end{aligned} \tag{5}$$

where $\phi_{\mathrm{CRLH}}(\omega)$ and $\phi_{\mathrm{DSE}}(\omega)$ are the insertion phase shifts of the original CRLH cell and the DSE component, respectively. d_{CRLH} and d_{DSE} are the lengths of the CRLH cell and the DSE component, respectively, and d_{total} is the total length of one CRLH cell and one DSE component.

Furthermore, the dispersion sensitivity of the CRLH-LWA with the DSE component can be derived as

$$\beta'_{\mathrm{CRLH-DSE}}(\omega) = \frac{\phi'_{\mathrm{CRLH}}(\omega) + \phi'_{\mathrm{DSE}}(\omega)}{d_{\mathrm{CRLH}} + d_{\mathrm{DSE}}}. \tag{6}$$

Consequently

$$\frac{\beta'_{\mathrm{CRLH-DSE}}(\omega)}{\beta'_{\mathrm{CRLH}}(\omega)} = \frac{1 + \phi'_{\mathrm{DSE}}(\omega)/\phi'_{\mathrm{CRLH}}(\omega)}{1 + d_{\mathrm{DSE}}/d_{\mathrm{CRLH}}}. \tag{7}$$

By (7), if the DSE component has both a sufficiently large phase change rate and a short length simultaneously, the CRLH-LWA with DSE components will have larger dispersion sensitivity than the original one, leading to a wider beam scanning range. In addition, considering practical requirements for the performance of wireless systems, the DSE component also needs to fulfill the following requirements.

1) The DSE component should satisfy the impedance matching condition in an as-wide-as-possible frequency band.
2) The phase change rate $\phi'_{\mathrm{DSE}}(\omega)$ of the DSE component has to be a positive constant a to guarantee the linearity of the DSE component, which is expressed by

$$\phi'_{\mathrm{DSE}}(\omega) = a. \tag{8}$$

3) The insertion phase shift $\phi_{\mathrm{DSE}}(\omega)$ of the DSE component must be $2k\pi$ (k is a positive integer) to retain the balanced frequency of the original LC-CRLH-LWA; thus, there is

$$\phi_{\mathrm{DSE}}(\omega_0) = 2k\pi. \tag{9}$$

Solving (8) and (9) and assuming $\phi_{\mathrm{DSE}}(0) = \phi_0$ leads to

$$\phi_{\mathrm{DSE}}(\omega) = a(\omega - \omega_0) + 2k\pi \tag{10}$$

$$a = \frac{\phi_{\mathrm{DSE}}(\omega_0) - \phi_0}{\omega_0}. \tag{11}$$

It is worth noting that although the above-mentioned requirements seem harsh, it can be easily achieved by a meander transmission line structure. According to [24] and [25], the meander line can be used as a kind of miniaturized phase shifter with excellent performances, such as broad bandwidth, short length, and large phase shift, which exactly fits the requirements of the DSE component.

III. Design of LC-CRLH-LWA With the DSE Component

A. LC-CRLH-LWA Without the DSE Component

In order to demonstrate the efficiency of the proposed DSE method, an LC-CRLH-LWA without the DSE component is designed at first. It is constituted by concatenating eight unit cells, as illustrated in Fig. 3(a) and (b).

As the 3-D hierarchical view shown in Fig. 3(a), the LC-CRLH-LWA is a triple-layer structure consisting of a dielectric slab with a sophisticated metallic structure printed on its lower surface, followed by an LC layer and a metal base. As the cross-sectional view illustrated in Fig. 3(b), there is a groove on the metal base surface forming a cavity, in combination with the dielectric slab where the LCs are located. In the cavity, the radio frequency (RF) waves propagate along the y-direction in a similar mode as in an inverted microstrip line. The bias dc voltage V_{dc} is applied on the LC layer through the metal base and the metallic structure printed on the dielectric slab to control the LC molecules' orientation. At the two terminals of the antenna, two inverted microstrip lines on the upper surface of the dielectric slab are transited to microstrips feeder lines on the lower surface of the dielectric slab through metallic via holes.

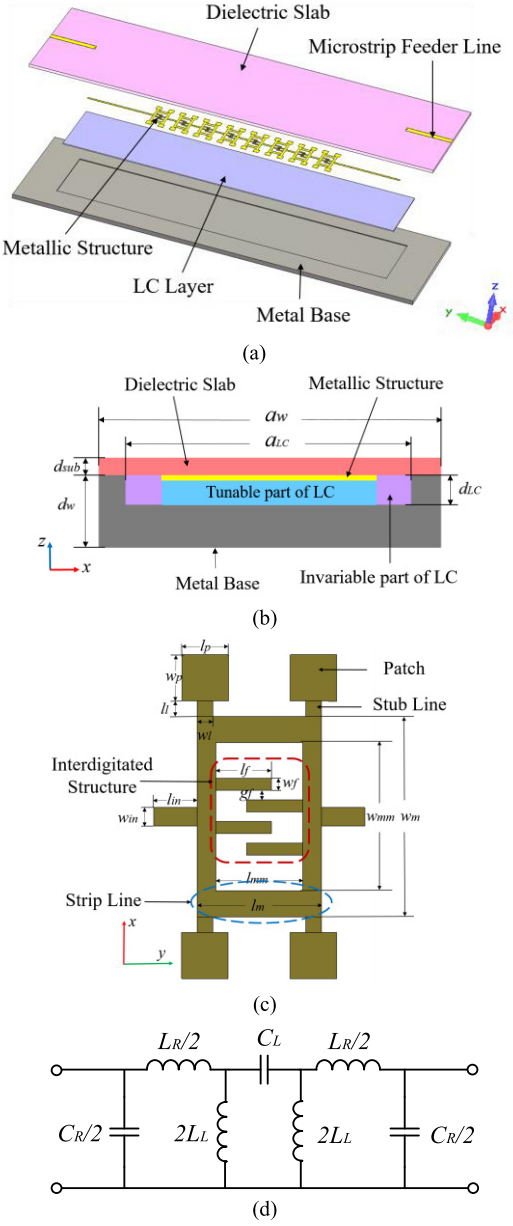

Fig. 3. Schematic of the LC-CRLH-LWA. (a) 3-D hierarchical view. (b) Cross-sectional view of unit cell. (c) Detailed geometry of the metallic structure. (d) Equivalent circuit of the CRLH unit cell.

TABLE I
SIMULATION PARAMETERS OF THE LC-CRLH-LWA

Parameters	l_m	w_m	l_{mm}	w_{mm}	l_{in}	w_{in}
Value(mm)	4	6.5	2.8	4.8	1.4	0.6
Parameters	l_l	w_l	l_p	w_p	l_f	w_f
Value(mm)	0.5	0.5	1.5	1.5	1.8	0.4
Parameters	g_f	a_w	a_{LC}	d_{sub}	dw	d_{LC}
Value(mm)	0.3	30	15.9	0.762	2.0	0.25

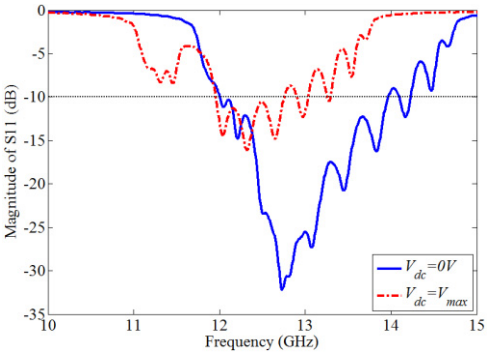

Fig. 4. Simulated magnitude of S_{11} of the LC-CRLH-LWA for the two extreme LC states. The solid line represents the $V_{\rm dc} = 0$ V state, while the dashed line corresponds to the $V_{\rm dc} = V_{\rm max}$ state.

The detailed pattern of the metallic structure printed on the dielectric slab is shown in Fig. 3(c). Its symmetrical configuration is similar to that in [26], but considerably modified to operate with the LCs in the Ku-band for the satellite communication application. The equivalent circuit of the CRLH unit cell is sketched in Fig. 3(d). The desired series capacitance C_L for the CRLH transmission line is realized by the interdigitated structure, while the shunt inductance L_L is obtained by the stub lines linked with square patches. The series shunt capacitance C_R is acquired by the metal structure and the metal base, while the series inductance L_R is achieved by the metallic stubs. Two strip lines are connected with the interdigitated structure for feeding the RF waves.

When the bias voltage $0 < V_{\rm dc} < V_{\rm max}$, the LCs' effective permittivity tensor is tuned between $\varepsilon_{r\perp}$ and $\varepsilon_{r//}$. In the simulations, $\varepsilon_{r\perp} = 2.43$ and $\varepsilon_{r//} = 3.22$ are used for LCs, which is derived from the material TUD-649 produced by Merck Corporation [15], while aluminum and copper are used for the metal base and the printed metallic structure, respectively. The relative permittivity of the dielectric slab is 3.66. In addition, in the simulations, the permittivity tensor of the LCs underneath the metallic structure is set to be tunable with the bias voltage, while the permittivity tensor of the residual LCs remains constant as shown in Fig. 3(b). CST MW Studio software package is used to validate the design model. The detailed simulation parameters of the model are listed in Table I.

When port1 is fed and port2 is terminated with a matched load, the simulated results of $|S_{11}|$ are plotted in Fig. 4. An overlapped passband from 12 to 12.75 GHz is achieved for the two extreme LCs states. Fig. 5 shows the normalized far-field patterns of the antenna for the two extreme LCs states at 12.4 GHz. It can be seen that the main beam direction scans from 0° to 30° as the LCs permittivity are tuned by the corresponding bias voltages $V_{\rm dc}$ from 0 V to $V_{\rm max}$.

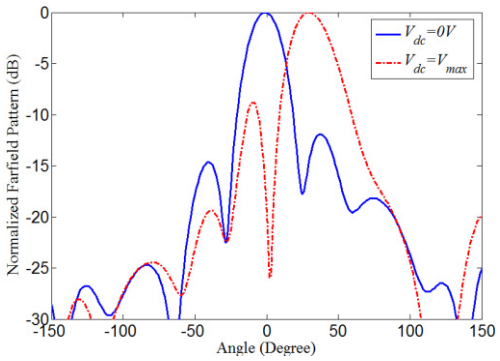

Fig. 5. Simulated radiation patterns at 12.4 GHz, where the solid line represents the $V_{\rm dc} = 0$ V state, while the dashed line corresponds to the $V_{\rm dc} = V_{\rm max}$ state.

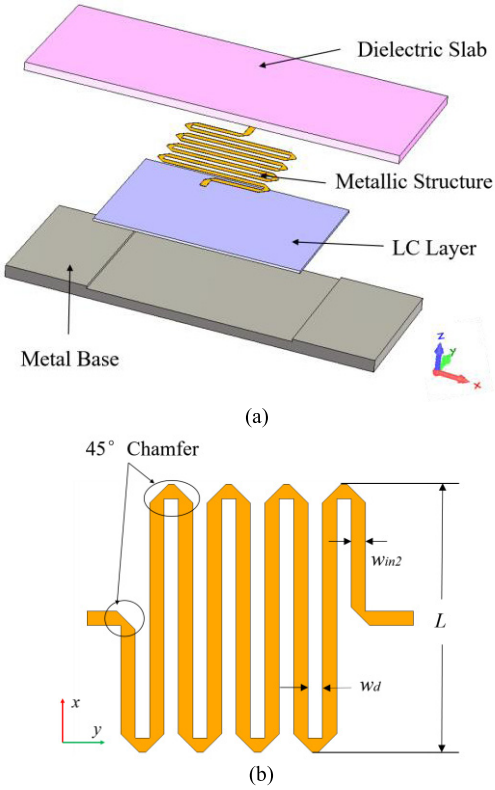

Fig. 6. Schematic of the LC-based meander line structure. (a) 3-D hierarchical view. (b) Detailed structure of the metallic meander line.

B. DSE Component Based on Meander Lines

As described in Section II, the meander line is a suitable candidate for a compact DSE component to enlarge the electrical beam scanning range of LC-CRLH-LWAs. Therefore, an LC-based meander-line structure with high dispersion sensitivity is designed as shown in Fig. 6(a). Similar to the LC-CRLH-LWA without DSE components in Section III-A, the LC-based meander-line DSE component consists of a dielectric slab with printed metallic meander-line structure on the lower face, followed with an LC layer and a metal base. As the detailed geometry of the meander-line structure shown in Fig. 6(b), the space between the adjacent strip lines w_d affects both the

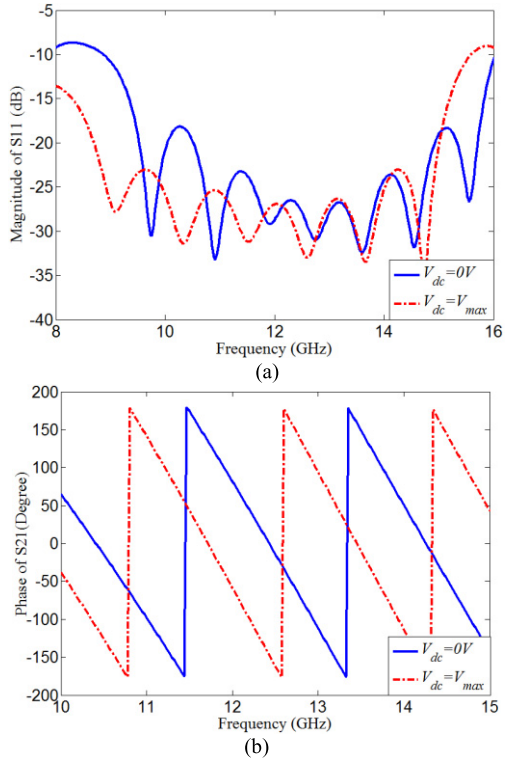

Fig. 7. (a) Simulated magnitude of $S11$ and (b) simulated phase of $S21$ of the LC-based meander line for the two extreme states of LCs. The solid line represents the $V_{\rm dc} = 0$ V state, while the dashed line corresponds to the $V_{\rm dc} = V_{\rm max}$ state.

return loss and the insertion loss. L is the length of the segment strip line, which determines the bandpass frequency. The width of the strip line $w_{\rm in2}$ is crucial for the operating frequency and the impedance matching. After optimization, the detailed parameters of the meander line are $w_d = w_{\rm in2} = 0.6$ mm and $L = 11.2$ mm. Compared to conventional ones, a 45° chamfer is devised at every corner of the meander line and is optimized to further reduce the occupied circuit area of the meander line.

The simulated S_{11} magnitude of the LC-based meander line is shown in Fig. 7(a). From 10.6 to 14.8 GHz, the structure shows good impedance matching for both two extreme states of the LCs (below –20 dB). The simulated results of the insertion phase shift are plotted in Fig. 7(b). It can be observed that the insertion phase shift provides linear frequency dependence, approaching 0° at 12.4 and 11.6 GHz for $V_{\rm dc} = 0$ V and $V_{\rm dc} = V_{\rm max}$, respectively. Such properties guarantee that both the linearity and the balanced frequency of the LC-CRLH-LWA will not be disturbed by adding the DSE components, as described in Section II.

C. LC-CRLH-LWA With the DSE Components

Combination of the above-designed LC-CRLH-LWA (Fig. 3) with the DSE component (Fig. 6) leads to a new type of LC-CRLH-LWA, as shown in Fig. 8. It is expected that the LC-CRLH-LWA with the DSE components will exhibit a higher dispersion sensitivity and, hence, a larger beam scanning range than the original one shown in Fig. 3.

Numerical simulations are conducted to demonstrate the performance of the LC-CRLH-LWA with the DSE components. The simulated dispersion curves of the LC-CRLH-LWA

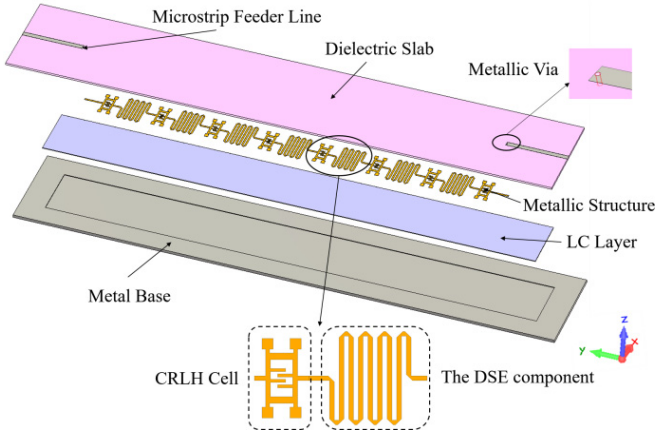

Fig. 8. Schematic of the LC-CRLH-LWA with the DSE components.

with and without the DSE components are depicted in Fig. 9 for comparison. It can be clearly seen that the dispersion curves of the LC-CRLH-LWA with the DSE components are much steeper than those without the DSE component, while the balanced conditions are well kept for both the two extreme states of LCs. This phenomenon validates that the inclusion of the DSE components can significantly enhance the dispersion sensitivity of the LC-CRLH-LWA, which verifies our theory highlighted in Section II.

The simulated radiation patterns of the antenna with the DSE components at 12.4 GHz for the maximum-biased state ($V_{\rm dc} = V_{\rm max}$) and the unbiased state ($V_{\rm dc} = 0$ V) of LCs are shown in Fig. 10(a). Accordingly, the main beam direction scans from 0° to 47° as the bias voltage increases from 0 V to $V_{\rm max}$, extended by more than 56%, which is much larger than that without the DSE component. The main lobe direction of the antenna as a function of the operating frequency is depicted in Fig. 10(b), where the results for the LC-CRLH-LWA without the DSE component are also plotted to facilitate comparison.

As displayed in Fig. 10(b), the antenna with the DSE components exhibits a larger beam scanning range than that without the DSE component in a quite wide frequency band. Fig. 11 shows the simulated results for the $_{11}$ magnitude of the LC-CRLH-LWA with the DSE components for the two extreme states of LCs. It can be seen that for both the two LCs' extreme states, the return loss is smaller than -10 dB in the frequency range from 12.1 to 12.75 GHz, which is suitable for the down link of the Ku-band satellite communication. The impedance-matching characteristics of the original LC-CRLH-LWA are well kept, on the account of the designed DSE component having an adequate low return loss within a board bandwidth, as depicted in Fig. 4.

In summary, compared to the structure without the DSE component as shown in Fig. 6, the LC-CRLH-LWA with DSE components (i.e., the LC-based meander-line structure) exhibits enhanced dispersion sensitivity, which leads to an enlarged scanning range from 30° to 47° while retaining the impedance-matching characteristics. These results perfectly confirm our theoretical predictions developed in Section II.

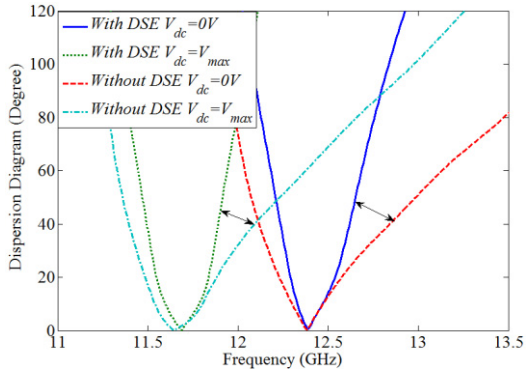

Fig. 9. Simulated dispersion curves of the LC-CRLH-LWA with and without the DSE components for the two extreme states of LCs. The blue and red lines represent the $V_{\rm dc} = 0$ V state, while the green and light blue lines correspond to the $V_{\rm dc} = V_{\rm max}$ state.

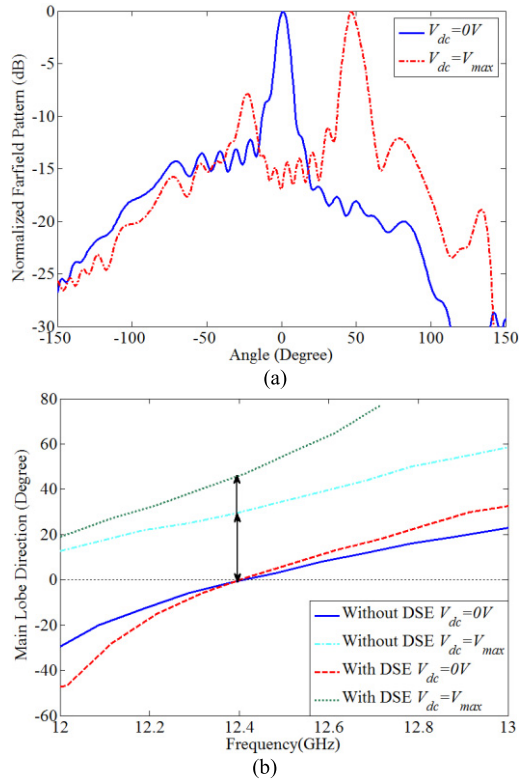

Fig. 10. (a) Simulated normalized far-field patterns. The solid line represents the $V_{\rm dc} = 0$ V state, while the dashed line corresponds to the $V_{\rm dc} = V_{\rm max}$ state LCs implying a beam scanning range of 47°. (b) Main lobe direction of the LC-CRLH-LWA with and without the DSE components as a function of operating frequency for the two extreme states of LCs. The blue and red lines represent the $V_{\rm dc} = 0$ V state, while the green and light blue lines correspond to the $V_{\rm dc} = V_{\rm max}$ state.

IV. Fabrication and Experimental Verification

In order to demonstrate our proposed theoretical and numerical results, two prototype samples for the LC-CRLH- LWAs with and without the DSE components are fabricated and tested experimentally. The photographs of the samples are shown in Fig. 12(a) and (b).

A Rogers 4350B-type substrate and 0603-type aluminum alloy are used for the dielectric slab and the metal base, respectively. A groove is milled into the metal base surface forming a cavity together with the Rogers substrate. Computer numerical control milling machine is used to obtain the groove with 0.25 mm depth. A coating of polyvinyl alcohol is put on the surface of the groove and rubbed to realize the LCs' director alignment along the y-direction. Aligned screw holes are embedded around the substrate and the metal base for fixation with screws to package the LCs and ensure the mechanical stability over time. Another two small holes in the diagonal of the substrate are constituted to inject the LCs into the cavity. Extra glue embraces the substrate and the metal base for the final packaging.

Compared to the existing LC microwave devices, components realized by the fabrication methodology in this paper feature low cost; compactness; ease of fabrication, design, and packaging; greater mechanical stability; and capability of handling high power.

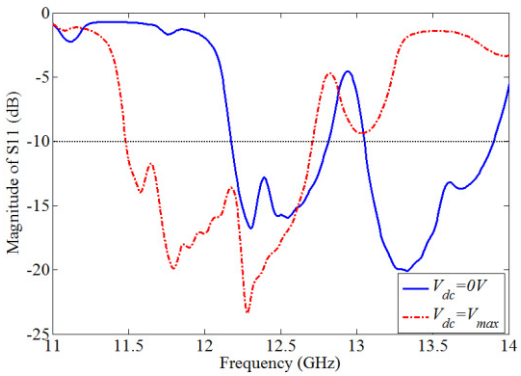

Fig. 11. Simulated magnitude of S_{11} of the LC-CRLH-LWA with the DSE components for the two extreme states of LCs. The solid line represents the $V_{\rm dc} = 0$ V state, while the dashed line corresponds to the $V_{\rm dc} = V_{\rm max}$ state.

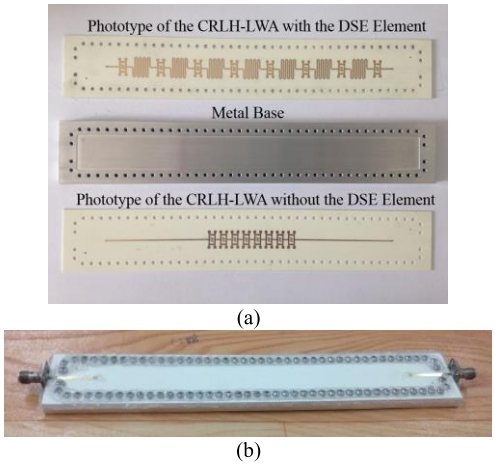

Fig. 12. Photographs of the fabricated LC-CRLH-LWA. (a) Inner structures. (b) Packaged sample.

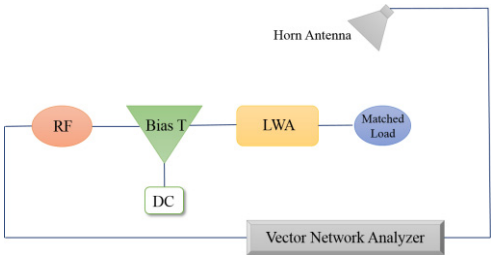

Fig. 13. Schematic of measurement system for the LC-CRLH-LWA.

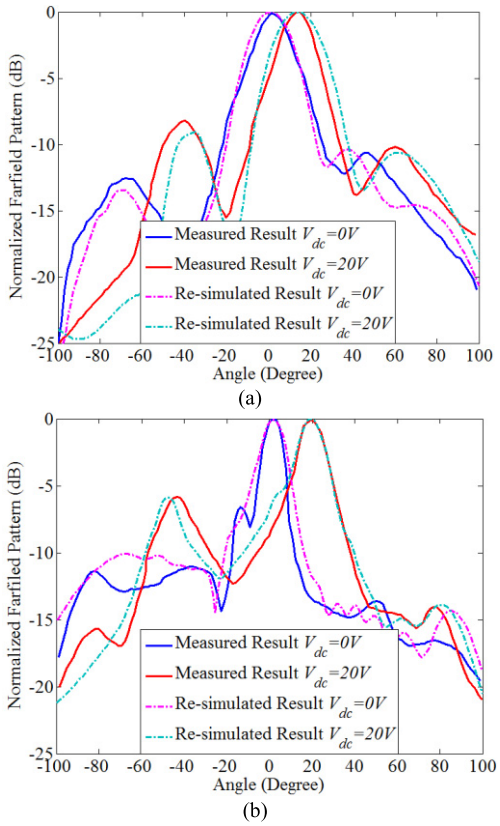

Fig. 14. Measured and resimulated normalized far-field patterns of the LC-CRLH-LWAs (a) without and (b) with the DSE components at 12.4 GHz. The solid line represents the measured results, while the dashed line corresponds to the resimulated results.

There are two differences between the fabricated samples and the simulation models. First, the LC material used in the experiment is different from the simulated one. The CDZSL-018-type LC material produced by BAYI Space LCD Company is chosen as a substitute in the experiments with the tunable effective permittivity of $\varepsilon_{r\perp} = 2.46$ and $\varepsilon_{r//} = 2.95$, and its loss tangent is 0.037. The second difference between simulations and measurements is the metal base. To reduce the fabrication cost, the LC-CRLH-LWAs with and without the DSE component share the same metal base, which leads to a groove of the antenna without the DSE component much longer than that in the simulations.

The measurement is conducted in a microwave anechoic chamber, and its setup is illustrated in Fig. 13. The LC-CRLH-LWA is fed by the electromagnetic waves from Agilent N5227A vector network analyzer through a Bias-T and terminated by a matched load. The biased voltage is applied to the LCs in the LWA through the Bias-T. The horn antenna works as a receiving antenna.

The measured normalized far-field patterns of the LC-CRLH-LWA without and with the DSE components at 12.4 GHz are shown in Fig. 14(a) and (b), for the two extreme states of the LCs. It can be seen that the LC-CRLH-LWA with the DSE components shows a larger beam scanning range than that without the DSE. However, it is also found that for both cases, the measured antenna beam scanning range is narrower than the simulated ones as shown in Figs. 5 and 10. This phenomenon can be explained by the fact that

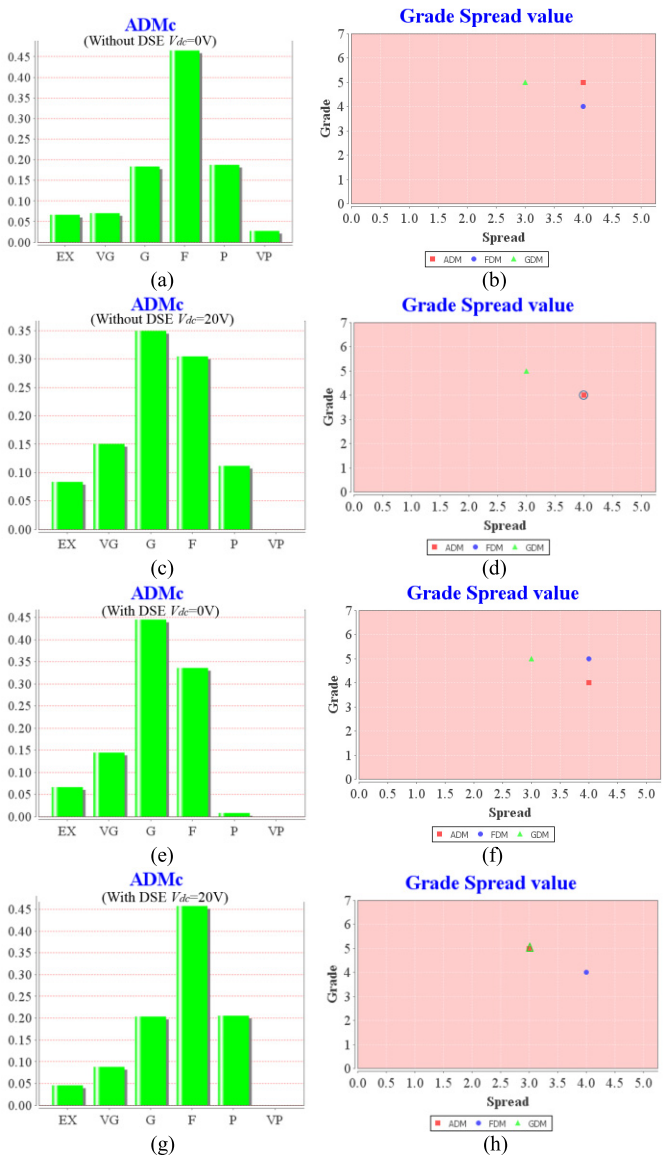

Fig. 15. Results of FSV technique. (a) ADM histogram and (b) grade spread chart of the LC-CRLH-LWA without DSE for V_{dc} = 0-V state. (c) ADM histogram and (d) grade spread chart of the LC-CRLH-LWA without DSE for V_{dc} = 20-V state. (e) ADM histogram and (f) grade spread chart of the LC-CRLH-LWA with DSE for V_{dc} = 0-V state. (g) ADM histogram and (h) grade spread chart of the LC-CRLH-LWA with DSE for V_{dc} = 20-V state.

the experimental LC yields a smaller tunability than those in the simulations. In the numerical analysis, in order to make a direct comparison between the performances of our designed antenna and previously reported works, we model the LC strictly referring to the experimental one of the Merck TUD-649 in [15]. This LC supports a strong tunability, but, unfortunately, we were not able to get it for our laboratory. Consequently, we have to choose the CDZSL-018-type LC as a substitute for our experiments to demonstrate the proposed idea. In order to confirm the above-mentioned reasoning, the simulations are repeated with the effective permittivity and loss tangent of the CDZSL-018 LC, and the results are also shown in Fig. 14(a) and (b) for comparison. It can be seen that the resimulated results coincide well with the measured results.

Furthermore, the feature selective validation (FSV) technique [27]–[29] is applied to provide a quantified and comprehensible evaluation on the measured and simulated results. In the case of LC-CRLH-LWAs, the amplitude difference measure value is expected to assess the similarity of the measured and simulated far-field patterns. The statistical amplitude difference measure (ADM) histograms by the FSV approach are obtained in Fig. 15(a), (c), (e), and (g) corresponding to the antennas without or with the DSE components for $V_{\rm dc} = 0$ V or $V_{\rm dc} = V_{\rm max}$ state. In all the cases, a strong similarity is revealed in the ADM histograms between simulations and measurements (Excellent + Very Good + Good + Fair > 80%). Moreover, the corresponding grade spread values are displayed in Fig. 15(b), (d), (f), and (h) for comprehensive quantification and visual indication [30], [31]. In all the cases, the grade and spread values of the ADM, the feature difference measure (FDM), and the global difference measure are between 4–5 and 3–4, respectively, thus indicating a poor to good agreement of the measured (GDM) and simulated far-field patterns. This result may well be accepted as good agreement between two plots, despite having some differences with respect to machining errors, instrumental errors, and noise.

V. Conclusion

A general design, fabrication, and packaging method of electrically tunable LC-CRLH-LWAs with enlarged beam scanning range is put forward. The LCs are packaged by PCB processing technology combined with the metal precision machining process, which makes the design of LC microwave components no longer limited by the microelectronics processing technology. Theoretical analyses demonstrate that the slope of dispersion curves of LC-CRLH-LWA is a critical factor to the beam scanning range. Afterward, a specific DSE component with high dispersion sensitivity and good impedance matching property is designed and added to an LC-CRLH-LWA to expand the electronic beam scanning range. Simulated results exhibit that the DSE method improves the beam scanning range from 30° to 47° for operating frequencies within the spectral band from 12.1 to 12.75 GHz, which is suitable for the down link of the Ku-band satellite communication. Measurements are conducted to confirm the theoretical and numerical results, and the FSV technique is utilized to assess the similarity between the experimental and simulated results. Furthermore, this fabrication technology makes LC components with low cost, mechanical stability, ease of manufacture, and flexible design. In conclusion, our novel beam scanning method and fabrication methodology of LC components are fully functional and highly effective.

Acknowledgment

The authors would like to thank the reviewers and editors for their constructive comments and suggestions, which have been valuable to improve this paper.

References

[1] J. L. Gomez-Tornero, F. D. Quesada-Pereira, and A. Alvarez-Melcon, "Analysis and design of periodic leaky-wave antennas for the millimeter waveband in hybrid waveguide-planar technology," *IEEE Trans. Antennas Propag.*, vol. 53, no. 9, pp. 2834–2842, Sep. 2005.

[2] J. Liu, D. R. Jackson, Y. Li, C. Zhang, and Y. Long, "Investigations of SIW leaky-wave antenna for endfire-radiation with narrow beam and sidelobe suppression," *IEEE Trans. Antennas Propag.*, vol. 62, no. 9, pp. 4489–4497, Sep. 2014.

[3] A. J. Martinez-Ros, J. L. Gomez-Tornero, and G. Goussetis, "Planar leaky-wave antenna with flexible control of the complex propagation constant," *IEEE Trans. Antennas Propag.*, vol. 60, no. 3, pp. 1625–1630, Mar. 2012.

[4] A. Mehdipour and G. V. Eleftheriades, "Leaky-wave antennas using negative-refractive-index transmission-line metamaterial supercells," *IEEE Trans. Antennas Propag.*, vol. 62, no. 8, pp. 3929–3942, Aug. 2014.

[5] W. Cao, Z. N. Chen, W. Hong, B. Zhang, and A. Liu, "A beam scanning leaky-wave slot antenna with enhanced scanning angle range and flat gain characteristic using composite phase-shifting transmission line," *IEEE Trans. Antennas Propag.*, vol. 62, no. 11, pp. 5871–5875, Nov. 2014.

[6] L. Cui, W. Wu, and D.-F. Fang, "Printed frequency beam-scanning antenna with flat gain and low sidelobe levels," *IEEE Antennas Wireless Propag. Lett.*, vol. 12, pp. 292–295, 2013.

[7] N. Apaydin, K. Sertel, and J. L. Volakis, "Nonreciprocal and magnetically scanned leaky-wave antenna using coupled CRLH lines," *IEEE Trans. Antennas Propag.*, vol. 62, no. 6, pp. 2954–2961, Jun. 2014.

[8] T. Kodera, D. L. Sounas, and C. Caloz, "Nonreciprocal magnetless CRLH leaky-wave antenna based on a ring metamaterial structure," *IEEE Antennas Wireless Propag. Lett.*, vol. 10, pp. 1551–1554, 2011.

[9] H. Paaso, A. Mammela, D. Patron, and K. R. Dandekar, "DoA estimation through modified unitary MUSIC algorithm for CRLH leaky-wave antennas," in *Proc. Int. Symp. IEEE Pers. Indoor Mobile Radio Commun. (PIMRC)*, London, U.K., Sep. 2013, pp. 311–315.

[10] H. V. Nguyen, S. Abielmona, and C. Caloz, "End-switched CRLH leaky-wave antenna with enhanced electronic full-space beam steering performance," in *Proc. 5th Eur. Conf. Antennas Propag.*, Rome, Italy, 2011, pp. 3501–3503.

[11] S. Bulja, D. Mirshekar-Syahkal, R. James, S. E. Day, and F. A. Fernandez, "Measurement of dielectric properties of nematic liquid crystals at millimeter wavelength," *IEEE Trans. Microw. Theory Techn.*, vol. 58, no. 12, pp. 3493–3501, Dec. 2010.

[12] I. C. Khoo, D. H. Werner, X. Liang, A. Diaz, and B. Weiner, "Nanosphere dispersed liquid crystals for tunable negative–zero–positive index of refraction in the optical and terahertz regimes," *Opt. Lett.*, vol. 31, no. 17, pp. 2592–2594, 2006.

[13] D. H. Werner, D.-H. Kwon, I.-C. Khoo, A. V. Kildishev, and V. M. Shalaev, "Liquid crystal clad near-infrared metamaterials with tunable negative-zero-positive refractive indices," *Opt. Express*, vol. 15, no. 6, pp. 3342–3347, 2007.

[14] F. Zhang, L. Kang, Q. Zhao, J. Zhou, X. Zhao, and D. Lippens, "Magnetically tunable left handed metamaterials by liquid crystal orientation," *Opt. Express*, vol. 17, no. 6, pp. 4360–4366, 2009.

[15] M. Roig, M. Maasch, C. Damm, and R. Jakoby, "Dynamic beam steering properties of an electrically tuned liquid crystal based CRLH leaky wave antenna," in *Proc. Int. Conf. Adv. Electromagn. Mater. Microw. Opt. (METAMATERIALS)*, Kongens Lyngby, Denmark, 2014, pp. 253–255.

[16] M. Roig, M. Maasch, C. Damm, and R. Jakoby, "Liquid crystal-based tunable CRLH-transmission line for leaky wave antenna applications at Ka-Band," *Int. J. Microw. Wireless Tech.*, vol. 6, pp. 325–330, Mar. 2014.

[17] M. Roig, M. Maasch, C. Damm, and R. Jakoby, "Electrically tunable liquid crystal based composite right/left-handed leaky-wave antenna at 26.7 GHz," in *Proc. 44th Eur. Microw. Conf. (EuMC)*, Rome, Italy, 2014, pp. 331–334.

[18] C. Damm, M. Maasch, R. Gonzalo, and R. Jakoby, "Tunable composite right/left-handed leaky wave antenna based on a rectangular waveguide using liquid crystals," in *IEEE MTT-S Int. Microw. Symp. Dig.*, May 2010, pp. 13–16.

[19] H. Lee, J. H. Choi, C. T. M. Wu, and T. Itoh, "A compact single radiator CRLH-inspired circularly polarized leaky-wave antenna based on substrate-integrated waveguide," *IEEE Trans. Antennas Propag.*, vol. 63, no. 10, pp. 4566–4572, Oct. 2015.

[20] F. Bigelli *et al.*, "Design and fabrication of a dielectricless substrate-integrated waveguide," *IEEE Trans. Compon., Packag., Manuf. Technol.*, vol. 6, no. 2, pp. 256–261, Feb. 2016.
[21] Q. Yang, X. Zhao, and Y. Zhang, "Composite right/left-handed ridge substrate integrated waveguide slot array antennas," *IEEE Trans. Antennas Propag.*, vol. 62, no. 4, pp. 2311–2316, Apr. 2014.
[22] C. Jin and A. Alphones, "Leaky-wave radiation behavior from a double periodic composite right/left-handed substrate integrated waveguide," *IEEE Trans. Antennas Propag.*, vol. 60, no. 4, pp. 1727–1735, Apr. 2012.
[23] Q. Yang, Y. Zhang, and X. Zhang, "X-band composite right/left-handed leaky wave antenna with large beam scanning-range/bandwidth ratio," *Electron. Lett.*, vol. 48, no. 13, pp. 746–747, Jun. 2012.
[24] S. Bulja and D. Mirshekar-Syahkal, "Meander line millimetre-wave liquid crystal based phase shifter," *Electron. Lett.*, vol. 46, no. 11, pp. 769–771, May 2010.
[25] J. Wu *et al.*, "Compact, low-loss, wideband, and high-power handling phase shifters with piezoelectric transducer-controlled metallic perturber," *IEEE Trans. Microw. Theory Techn.*, vol. 60, no. 6, pp. 1587–1594, Jun. 2012.
[26] C.-Y. Liu, Q.-X. Chu, and J.-Q. Huang, "A planar D-CRLH transmission line structure and its application to leaky-wave antenna," in *Proc. Int. Symp. Antennas Propag. EM Theory (ISAPE)*, Guangzhou, China, 2010, pp. 345–348.
[27] *Standard for Validation of Computational Electromagnetics Computer Modeling and Simulation—Part 1, 2*, IEEE Standard P1597, 2008.
[28] A. P. Duffy, A. J. M. Martin, A. Orlandi, G. Antonini, T. M. Benson, and M. S. Woolfson, "Feature selective validation (FSV) for validation of computational electromagnetics (CEM). Part I—The FSV method," *IEEE Trans. Electromagn. Compat.*, vol. 48, no. 3, pp. 449–459, Aug. 2006.
[29] A. Orlandi, A. P. Duffy, B. Archambeault, G. Antonini, D. E. Coleby, and S. Connor, "Feature selective validation (FSV) for validation of computational electromagnetics (CEM). Part II—Assessment of FSV performance," *IEEE Trans. Electromagn. Compat.*, vol. 48, no. 3, pp. 460–467, Aug. 2006.
[30] A. Orlandi, G. Antonini, C. Ritota, and A. P. Duffy, "Enhancing feature selective validation (FSV) interpretation of EMC/SI results with grade-spread," in *Proc. IEEE Int. Symp. (EMC)*, Aug. 2006, pp. 362–367.
[31] B. Archambeault, A. P. Duffy, and A. Orlandi, "Using the feature selective validation technique to compare data sets," in *Proc. IEEE Int. Symp. (EMC)*, Aug. 2009, pp. 248–253.

Shuang Ma received the bachelor's and master's degrees in microwave engineering from the Harbin Institute of Technology, Harbin, China, in 2012 and 2014, respectively, where she is currently pursuing the Ph.D. degree with the Department of Microwave Engineering.

Her current research interests include beam-steering antenna, active frequency selective surface, and tunable microwave device and antenna.

Ms. Ma was an award recipient from the IEEE 5th Global Symposium on Millimeter Waves, Harbin, China, in 2012, the *International Journal of Security and its Applications* in 2013, and the 17th Biennial Conference on Electromagnetic Field Computation, Miami, FL, USA, in 2016.

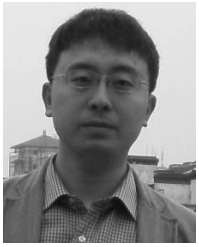

Guo-Hui Yang (S'07–M'09) received the B.S. degree in telecommunication, the M.S. degree in instrument science and technology, and the Ph.D. degree in electromagnetics from the Harbin Institute of Technology, Harbin, China, in 2003, 2006, and 2009, respectively.

Since 2009, he has been with the Department of Microwave Engineering, Harbin Institute of Technology, where he is currently an Associate Professor. His current research interests include RF micro-electromechanical systems device, tunable antenna, frequency selective surface, electromagnetic compatibility, and finite-difference time domain.

Daniel Erni (S'88–M'93) received the Diploma degree in electrical engineering from the University of Applied Sciences Rapperswil, Rapperswil-Jona, Switzerland, in 1986, and the Diploma degree in electrical engineering and the Ph.D. degree from ETH Zürich, Zürich, Switzerland, in 1990 and 1996, respectively.

Since 1990, he has been with the Laboratory of Electromagnetic Fields and Microwave Electronics, ETH Zürich, where he was the Founder from 1995 to 2006 and the Head of the Communication Photonics Group. Since 2006, he has been a Full Professor of general and theoretical electrical engineering with the University of Duisburg–Essen, Duisburg, Germany. On the system level, he has pioneered the introduction of numerical structural optimization into dense integrated optics device design. His current research interests include advanced data transmission schemes (i.e., O-MIMO) in board-level optical interconnects, optical on-chip interconnects, ultradense integrated optics, nanophotonics, plasmonics, quantum optics, and optical and electromagnetic metamaterials, with special focus on biomedical engineering, namely, for advanced RF excitation schemes in magnetic resonance imaging.

Dr. Erni is a Fellow of the Electromagnetics Academy. He is a member of the Center for Nanointegration Duisburg–Essen, the Applied Computational Electromagnetics Society, the Swiss Physical Society, the German Physical Society, and the Optical Society of America. He is an Associated Member of the Swiss Electromagnetics Research Center. He is a member of the Editorial Board of the *Journal of Computational and Theoretical Nanoscience*.

Fan-Yi Meng (S'07–M'09–SM'15) received the B.S., M.S., and Ph.D. degrees in electromagnetics from the Harbin Institute of Technology (HIT), Harbin, China, in 2002, 2004, and 2007, respectively.

Since 2007, he has been with the Department of Microwave Engineering, HIT, where he is currently a Professor. He has coauthored four books, 40 international refereed journal papers, over 20 regional refereed journal papers, and 20 international conference papers. His current research interests include antennas, electromagnetic and optical metamaterials, plasmonics, and electromagnetic compatibility.

Dr. Meng was a recipient of several awards, including the 2013 Top Young Innovative Talents of Harbin Institute of Technology, the 2013 CST University Publication Award, the 2010 Award of Science and Technology from the Heilongjiang Province Government of China, the 2010 Microsoft Cup IEEE China Student Paper Contest Award, two Best Paper Awards from the National Conference on Microwave and Millimeter Wave, China, in 2009 and 2007, the 2008 University Excellent Teacher Award of the National University of Singapore, the 2007 Excellent Graduate Award of Heilongjiang Province of China, and the Outstanding Doctor Degree Dissertation Award of the Harbin Institute of Technology.

Lei Zhu received the Ph.D. degree in electromagnetics from the Harbin Institute of Technology, Harbin, China, in 2014.

Since 2004, she has been with the Communication and Electronics Engineering Institute, Qiqihar University, Qiqihar, China, where she is currently an Associate Professor. She has coauthored two books and has authored or coauthored over 30 international and regional refereed journal papers. Her current research interests include electromagnetic and optical metamaterials, graphene, all-dielectric metamaterial, antenna design, and microwave devices.

Qun Wu (M'93–SM'05) received the B.Sc. degree in radio engineering, the M.Eng. degree in electromagnetic fields and microwaves, and the Ph.D. degree in communication and information systems from the Harbin Institute of Technology (HIT), Harbin, China, in 1977, 1988, and 1999, respectively.

He was a Visiting Professor with Seoul National University, Seoul, South Korea, from 1998 to 1999, the Pohang University of Science and Technology, Pohang, South Korea, from 1999 to 2000, and the National University of Singapore, Singapore, from 2003 to 2010. Since 1990, he has been with the School of Electronics and Information Engineering, HIT, where he is currently a Professor and the Head of the Department of Microwave Engineering. He is also a Director of the Center for Microwaves and Electro Magnetic Compatibility. He has authored or coauthored several books and over 100 international and regional refereed journal papers. His current research interests include electromagnetic compatibility, metamaterials, and antennas.

Dr. Wu received the Science and Technology Award from the Heilongjiang Provincial Government in 2010. He is a member of the Microwave Society of the Chinese Institute of Electronics. He is a Technical Reviewer for several international journals. He is also a Vice-Chair of the IEEE Harbin Section, and a Chair of the IEEE Harbin EMC/AP/MTT Joint Society Chapter. He was a Chair or a Member with the TPC of international conferences many times. He was also invited to give a keynote report or invited papers in some international conferences many times.

Jia-Hui Fu (M'07–SM'16) received the B.S. degree in electronics and communication engineering, the M.S. degree in electromagnetic fields and microwave technology, and the Ph.D. degree in communication and information systems engineering from the Harbin Institute of Technology (HIT), Harbin, China, in 1998, 2000, and 2005, respectively.

Since 2007, he has been with the Department of Microwave Engineering, HIT, where he is currently a Professor. His current research interests include microwave and millimeter-wave circuits, left-handed medium, microelectromechanical systems, and electromagnetic compatibility.